

## Meter-Scale Seafloor Geodetic Measurements Obtained from Repeated Multibeam Sidescan Surveys

John B. DeSanto & David T. Sandwell


To cite this article: John B. DeSanto & David T. Sandwell (2019): Meter-Scale Seafloor Geodetic Measurements Obtained from Repeated Multibeam Sidescan Surveys, Marine Geodesy, DOI: [10.1080/01490419.2019.1661887](https://doi.org/10.1080/01490419.2019.1661887)

To link to this article: <https://doi.org/10.1080/01490419.2019.1661887>



Accepted author version posted online: 04 Sep 2019.  
Published online: 04 Oct 2019.




[Submit your article to this journal](#) 



Article views: 7



[View related articles](#) 



[View Crossmark data](#) 



# Meter-Scale Seafloor Geodetic Measurements Obtained from Repeated Multibeam Sidescan Surveys

John B. DeSanto\* and David T. Sandwell

Scripps Institution of Oceanography, University of California San Diego, La Jolla, California, USA

## ABSTRACT

We calibrate a technique to use repeated multibeam sidescan surveys in the deep ocean to recover seafloor displacements greater than a few meters. Displacement measurements from seafloor patches (3 km by 20 km) on the port and starboard side of the ship are used to estimate vertical and across-track displacement. We present displacement measurements from a survey of the Ayu Trough southwest of the Marianas Trench using a 12 kHz multibeam. Vertical and across-track displacement errors for the 12 kHz multibeam sonar are typically 0–2 m with RMS uncertainties of 0.25–0.67 m in the across-track and 0.37–0.75 m in the vertical as determined by 3-way closure tests. The uncertainty of the range-averaged sound velocity is a major error source. We estimate that variations in the sound velocity profile, as quantified using expendable bathythermographs (XBTs) during data collection, contribute up to 0.3 m RMS uncertainty in the across-track direction and 1.6 m RMS uncertainty in the vertical direction.

## ARTICLE HISTORY

Received 5 March 2019

Accepted 13 August 2019

## KEYWORDS

Multibeam sonar; Seafloor positioning; Seafloor sonar image

## Introduction

Among the great geodetic challenges in Earth science is the problem of seafloor geodesy (Davis et al. 2012). Offshore earthquakes, volcanoes, and landslides can cause displacements on the meter scale or larger but are difficult to measure directly because the microwave signals that enable the collection of GPS and InSAR data cannot penetrate deeper than a few millimeters in seawater. As a result, specialized tools have been developed specifically to measure displacement on the seafloor, the most accurate of which are GPS-Acoustic and Bottom Pressure Recorders (Burgmann and Chadwell 2014). While these measurements are accurate to the centimeter scale, they are limited in that they are point measurements. Another instrument that may be used for seafloor geodetic application is the multibeam sonar, which collects bathymetry measurements in a broad swath beneath a research vessel.

**CONTACT** John B. DeSanto  [jdesanto@uw.edu](mailto:jdesanto@uw.edu)  University of California San Diego, Scripps Institution of Oceanography, La Jolla, CA 92093-0021, USA

\*John B. DeSanto now works at the Department of Earth and Space Sciences at the University of Washington, Seattle, WA.

Multibeam data are collected in “pings,” which consist of chirp pulses emitted by the sonar; reflections of a single pulse from the seafloor are logged before another pulse is emitted. The fundamental data we consider is the amplitude time series of each echo. For the remainder of this paper we shall refer to these as “sidescan” data since they are analogous to data collected by towed sidescan sonars, although it is important to clarify that these data are collected by a hull-mounted sonar rather than a towed sonar. Each ping consists of many points of amplitude, each with a unique look angle  $\theta$ , measured from vertical, and range  $\rho$ , the distance between the sonar and the point on the seafloor from which the echo reflected. For 12 kHz multibeam sonars, the slant range resolution is 11.25 m even in depths  $>3$  km. Amplitude points in a single ping are arranged roughly across track; we log the position of each ping with a value called the azimuth, the along-track distance from a shared reference point.

The method for measuring seafloor displacement with a multibeam sonar involves collecting repeated surveys of a patch of seafloor. Displacement between the surveys may be calculated via the normalized cross-correlation between surveys. The offset that yields the peak correlation coefficient is our desired measurement. The precision of a displacement calculated in this way is a sub-pixel fraction of the data resolution; a 12 kHz multibeam sonar has a bathymetry resolution on the order of 100–150 m for seafloor depths of  $\sim 3000$  m, so it is possible to resolve displacements on the order of 10 m. However, the sidescan data collected alongside bathymetry should be able to resolve displacements on the order of 1.125 m given its slant range resolution, a theoretical improvement of an order of magnitude over what is possible with bathymetry. This is less accurate than the displacements measurable using GPS-Acoustic or Bottom Pressure Recorders, but the multibeam sonar offers superior areal coverage and the meter resolution that may be achieved with sidescan is still sufficient to measure surface displacements from earthquakes  $>M_w$  7.0 or from submarine slope failures.

Previous studies have employed differential multibeam bathymetry to measure the seafloor displacement across the Japan Trench due to 2011  $M_w$  9.0 Tohoku-Oki earthquake in the regions offshore Miyagi (Fujiwara et al. 2011) and Sanriku (Fujiwara et al. 2017). These studies were able to identify the distribution of surface displacement with an accuracy on the order of 3–20 m. A study by DeSanto, Sandwell, and Chadwell (2016) proposed using digital image correlation on sidescan data collected simultaneously with multibeam bathymetry. The theoretical displacement resolution obtained from image correlation of sidescan data should be superior to that obtained from multibeam bathymetry because the resolution of sidescan is constant in slant range and thus independent of seafloor depth, in contrast

with multibeam bathymetry resolution, which becomes coarser in deeper waters. In addition, the sidescan data are less sensitive to roll biases than multibeam bathymetry. The DeSanto, Sandwell, and Chadwell (2016) study estimated a displacement precision of 0.75 m in the range dimension by analyzing legacy multibeam sidescan data from cruises in offshore Cascadia and Southern California. However, that study was unable to quantify the contribution of the correlation algorithm, navigation, and sound speed profile to the measurement uncertainty or how these uncertainties are impacted by survey design.

There are few requirements to be able to collect a displacement measurement using sonar data. The key experiment design involves returning to a previously surveyed region to collect a second data set of bathymetry and sidescan utilizing the same geometry as the older survey. In order to facilitate a valid cross-correlation between the reference and repeat surveys, we need sufficient information about the ship location and sound velocity profile for both surveys. The ship location is required to properly locate any patch of seafloor in space since the research vessel acts as the reference from which ranges are measured. Ideally the ship navigation has been post-processed using a technique such as Precise Point Positioning (PPP) as shown in DeSanto, Chadwell, and Sandwell (2018) to achieve an accuracy of 6 cm in the horizontal components and 14 cm in the vertical component. An appropriate sound velocity profile is required to properly perform ray-tracing when solving for the range of any sonar echo; poor constraints on the sound velocity can result in up to a few meters of range error as well as a poorly constrained look angle.

We seek to clarify the accuracy of displacement measurements from repeated sidescan surveys attainable given a wide variety of acquisition parameters. Some parameters, such as the ship speed and seafloor depth, influence the along-track sounding density on the seafloor with slower speeds and shallower depths allowing for a greater sounding density and thus more precise measurement (Kongsberg 2011). Sonar frequency and bandwidth affect sounding density in the across-track direction but also influences the swath width, with higher frequencies reducing the range of look angles from which data may be collected with an acceptable noise level. The track separation of the repeated tracks may play a significant role as the different ship locations will modify the range and look angle to reflectors on the seafloor between tracks as explained in DeSanto, Sandwell, and Chadwell (2016). In a similar fashion, heading variations during data collection influence the sounding density on the seafloor, with more stable surveys yielding more consistent sounding density. The quality of our knowledge of the ship position during acquisition places bounds on how well we may locate a patch of seafloor due to the sonar ranges being

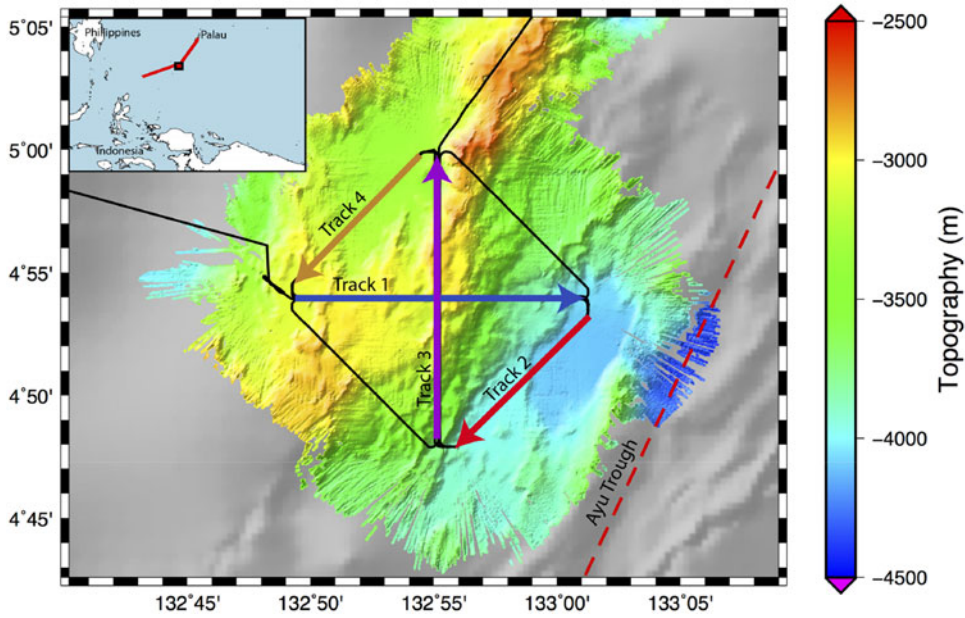


**Figure 1.** Topography collected during the RR1605 cruise (colored). Regional topography from before the cruise shown in the gray shaded background. Regional context of the cruise shown in inset map.

relative to the vessel. We also seek to quantify the uncertainties introduced to the data from perturbations of the sound velocity profile.

In this study, we consider data from the Roger Revelle, 2016, Leg 5 (RR1605) cruise. We performed a calibration survey during the RR1605 cruise in 2016, which consisted of five repeating multibeam surveys collected near the Ayu Trough  $\sim 200$  nautical miles southwest of Palau. The Ayu Trough is a slow spreading center denoting the southern plate boundary between the Philippine Sea Plate and the Caroline Sea Plate (Weissel and Anderson 1978). The plate motion across this boundary is difficult to resolve; marine seismic studies estimate the spreading rate to be 3.5–9.1 mm/yr based upon sediment thicknesses and sedimentation rates (Fujiwara et al. 1995; Hong and Lee 2002). The seafloor in this region is  $\sim 3000$ – $4000$  m deep and has a topographic fabric oriented approximately North-South, reflecting the plate boundary between the Philippine and Caroline Sea Plates. The survey area contains both a rough and reflective topographic high as well as a smoother topographic low.

The RR1605 experiment consists of repeated surveys consisting of four tracks (Figures 1 and 2): Track 1 is 12 nautical miles long and oriented due East with a heading of  $090^\circ$ . Track 2 is 8 nautical miles long and oriented Southwest with a heading of  $225^\circ$ . Track 3 is 12 nautical miles long and oriented due North with a heading of  $000^\circ$ , forming a cross with Track 1. Track 4 is an 8 nm long diagonal track similar to Track 2 with a heading

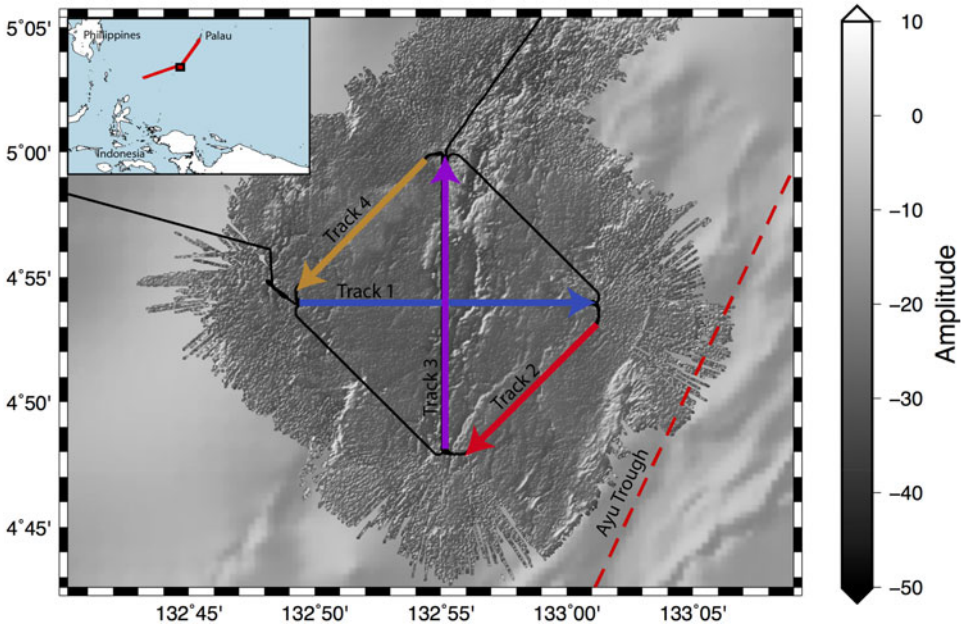


**Figure 2.** Sidescan collected during the RR1605 cruise. Regional topography from before the cruise shown in the gray shaded background. Regional context of the cruise shown in inset map.

of  $225^\circ$ , and connects the end of Track 3 with the start of Track 1 to form a closed loop. Tracks 1 and 3 were collected at a speed of 6 knots and have across-track separations varying from 0 to 300 m across track. Track 2 was collected at a speed of 4 knots and Track 4 was collected at a speed of 8 knots. Neither diagonal track has a variable track separation between surveys. Diagonal tracks in the Northeast and Southwest quadrants of the survey were collected once in order to facilitate a survey of Track 1 conducted with an opposite heading. Five repeated surveys were conducted in total, but because of the opposite heading survey of Track 1, only Track 3 has five true repeats. Tracks 1, 2, and 4 have four repeats each that we will consider in this study.

### Processing methods

The data used to obtain a seafloor displacement measurement consists of two multibeam sonar tracks that have been collected in the same area at different times. These tracks are close repeats with similar heading and location, and are ideally collected at the same speed with similar instruments so that they have comparable data density. Although each ping contains bathymetry and sidescan information, sidescan data have a finer resolution than the bathymetry. This difference in sampling means we must interpolate bathymetry data for an appropriate model of range and

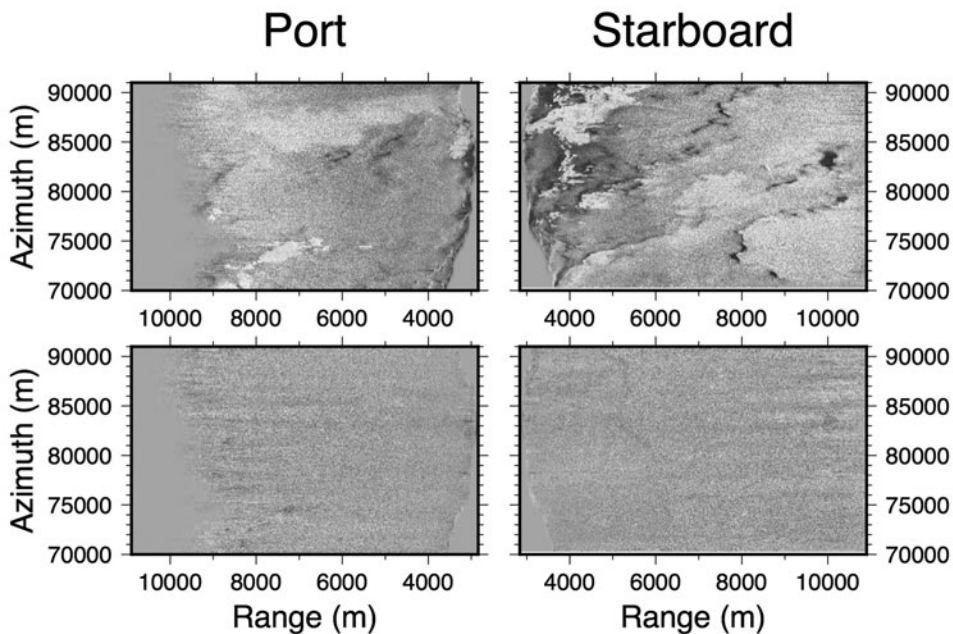


**Figure 3.** Sum (upper) and difference (lower) of two repeated sidescan sonar surveys of Track 3. The port and starboard sidescan data are plotted separately.

look angle (required to correct the sidescan range for baseline separations between the reference and repeat tracks) for sidescan amplitudes. Thus, the zeroth step for the sidescan processing is to process the bathymetry; we do so using the MB-System software (Caress and Chayes 2015). At this stage, we implement appropriate sound velocity profiles, tidal corrections, and navigation corrections if possible.

Data processing for the sidescan tracks follows the methodology described in DeSanto, Sandwell, and Chadwell (2016). First, we rotate the repeated tracks into a consistent coordinate frame of range and azimuth, correcting for across-track and heading deviations from a reference ship track. Second, we create grid files of sidescan amplitude as a function of range and azimuth. The sum and difference of an example pair of gridded sidescan surveys from Track 3 of the RR1605 experiment is shown in Figure 3. The sum of the sidescan grids shows the detailed sidescan of the seafloor while the difference resembles a random noise distribution, showing that a cross-correlation between the reference and repeat is well-founded. The range displacement of the port and starboard grids is computed independently by solving for the pixel offset that yields the maximum of a normalized cross correlation function, yielding a single displacement for each side. After estimating the port and starboard range displacements  $\rho$ , we may derive an expression for the average displacement  $u$  as a function of look angle  $\theta$  in a geographical coordinate frame by

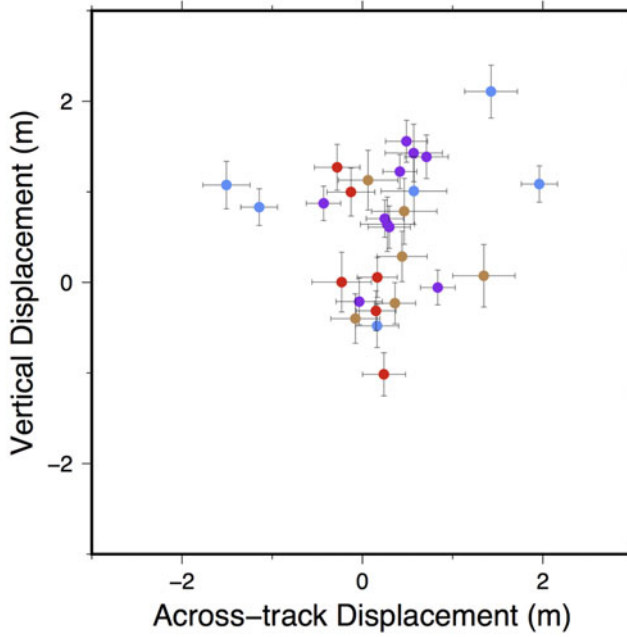


**Figure 4.** Displacement estimates between repeated sidescan sonar surveys. Colored points denote different tracks in the cruise: blue denotes Track 1, red Track 2, purple Track 3, and orange Track 4.

considering the geometry of the swath:

$$\begin{aligned} u_{\text{acrosstrack}} &= \frac{1}{2\theta_{\text{max}}} \int_{-\theta_{\text{max}}}^{\theta_{\text{max}}} \rho(\theta) \sin\theta \partial\theta \\ u_{\text{vertical}} &= \frac{1}{2\theta_{\text{max}}} \int_{-\theta_{\text{max}}}^{\theta_{\text{max}}} \rho(\theta) \cos\theta \partial\theta \end{aligned} \quad (1)$$

The cross correlation analysis yields one range displacement estimate for each of the port and starboard sides of the swath, so  $\rho(\theta)$  resembles a step function. Making this assumption, we may evaluate the above integrals as:

$$\begin{aligned} u_{\text{acrosstrack}} &= \frac{1 - \cos\theta_{\text{max}}}{2\theta_{\text{max}}} (\rho_{\text{starboard}} - \rho_{\text{port}}) \\ u_{\text{vertical}} &= \frac{\sin\theta_{\text{max}}}{2\theta_{\text{max}}} (\rho_{\text{starboard}} + \rho_{\text{port}}) \end{aligned} \quad (2)$$

The maximum look angle of a 12 kHz multibeam sonar is  $75^\circ$ , but we only consider data with a look angle less than  $65^\circ$  due to the higher noise at higher look angles. Assuming  $\theta_{\text{max}} = 65^\circ$ , the expressions for  $u$  evaluate to:

$$\begin{aligned} u_{\text{acrosstrack}} &\approx 0.25(\rho_{\text{starboard}} - \rho_{\text{port}}) \\ u_{\text{vertical}} &\approx 0.4(\rho_{\text{starboard}} + \rho_{\text{port}}) \end{aligned} \quad (3)$$



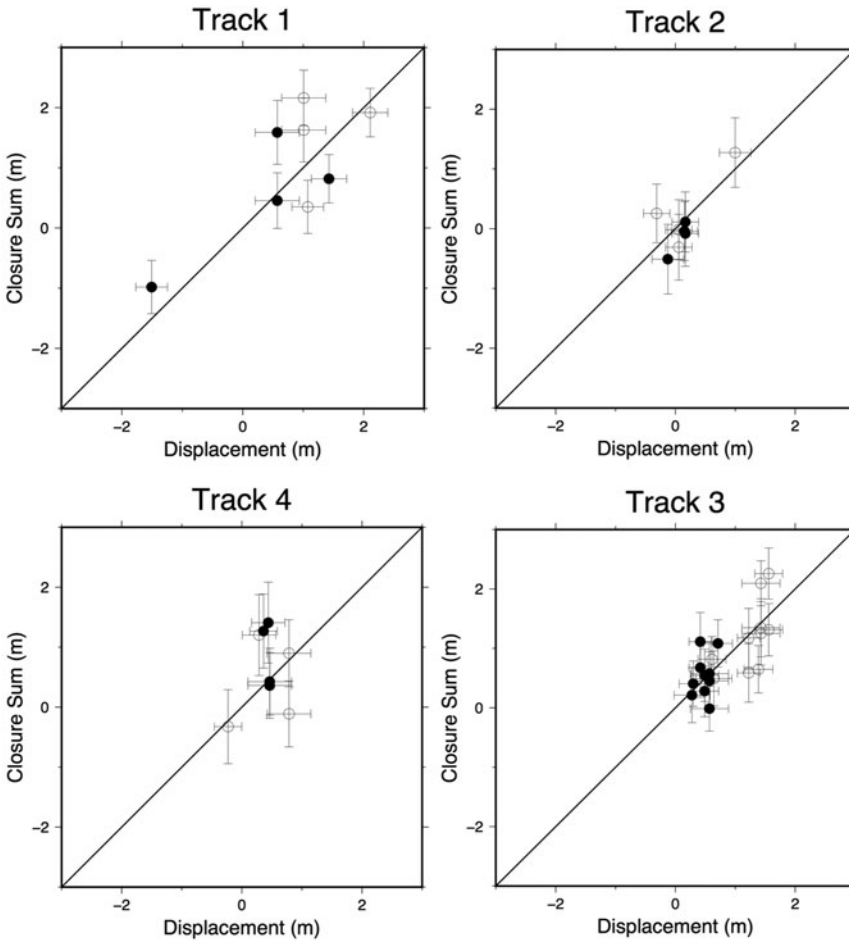


**Figure 5.** Closure of across-track (filled points) and vertical (open points) displacements, sorted by track. Vertical axis plots the sum of two displacement measurements while the horizontal axis plots the displacement that closes the loop. The line  $y = x$  denotes perfect closure.

### RR1605 displacement results

Displacements measured between every valid combination of repeated surveys are plotted in Figure 4, colored according to ship track. Error bars are calculated according to the reduced  $\chi^2$  values computed by the peak-fitting algorithm, and agree with the precision reported in DeSanto, Sandwell, and Chadwell (2016). Correlation coefficients associated with these displacements range from 0.4 to 0.6. Excluded are displacement measurements between repeated surveys of Track 1 and the opposite heading survey of Track 1, which produced correlation coefficients of 0.13–0.15 and subsequently measurements with far larger uncertainty. The vertical displacement measured in all tracks varies within 2 m, but the across-track displacement has a variance dependent on track.

**Table 1.** RMS values of mis-closures of loops of displacement measurements between repeated sidescan sonar surveys, sorted by track.

Track	Ship speed (knots)	RMS across-track mis-closure (m)	RMS vertical mis-closure (m)
1	6	0.65	0.75
2	4	0.25	0.37
3	6	0.33	0.45
4	8	0.67	0.65

A method by which we may assess the accuracy of these displacement 12 estimates is by forming closed loops of horizontal and vertical offsets from surveys in subsets of three or more. If no random noise is introduced into the measurements during the data processing, the displacement between any two surveys should be predictable using the sum of displacements obtained using an independent survey as a reference or repeat. We form closed loops using every possible combination of survey triplets for each of the four RR1605 tracks. Because Tracks 1, 2, and 4 have four repeated surveys each, there are four possible combinations of triplets for the closure tests. In contrast, Track 3 has five repeated surveys, which yields 10 possible combinations of triplets. The different number of triplets for the tracks is reflected in [Figure 5](#).

Closure test results are plotted in [Figure 5](#) separated by track, with the displacement between two surveys plotted on the horizontal axis and the prediction from the other displacements in the loop plotted on the vertical axis. Darker points correspond to across-track displacements while lighter points correspond to vertical displacements. In this configuration, points that plot closer to the line denoted by  $y = x$  are considered more accurate. [Table 1](#) displays the RMS of closure differences for the across-track and vertical displacement estimates associated with each track. The track with the most consistent measurements is Track 2 while the tracks with the least consistent measurements are Tracks 1 and 4. Tracks 1 and 3 (blue and purple, respectively) were collected at a speed of 6 knots and variable baseline, Track 2 (red) was collected at a speed of 4 knots, and Track 4 (orange) was collected at a speed of 8 knots. Track 1 displacements show the largest range of mis-closure while Track 2 displacements show the smallest range. At first glance, this lends credence to the hypothesis that data collected at a slower ship speed is of higher fidelity in that the slowest track (Track 2) yielded the most consistent results, but there is also rough equivalence in the spread of mis-closure between the Track 1 data collected at 6 knots and the Track 4 data collected at 8 knots.

We analyze the horizontal and vertical displacements measured between RR1605 surveys as a function of track separation. [Figure 6](#) shows no discernible dependence of displacement on track separation, implying that precise displacement measurements may be obtained even from tracks that are separated by as much as 300 meters. We interpret this as evidence that

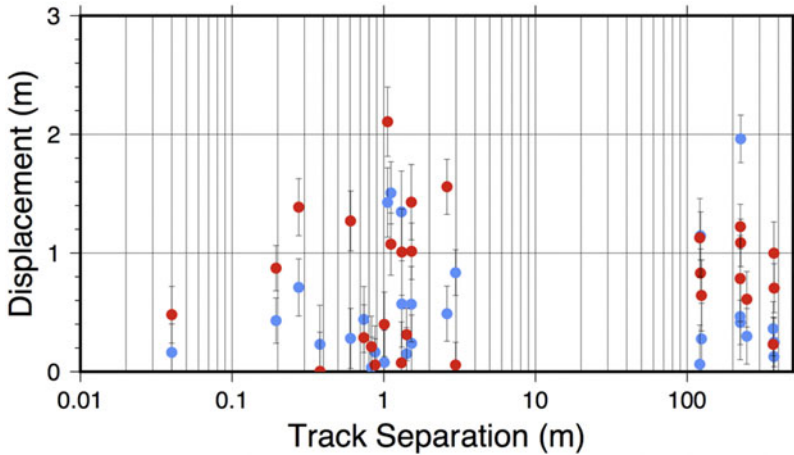


**Figure 6.** Across-track (blue) and vertical (red) displacement estimates between repeated side-scan surveys, plotted according to track separation.

the repeated tracks have been successfully translated to a common reference track, eliminating range errors that would arise due to ship sway from the reference.

### Effects of layered ocean sound velocity

Our analysis thus far has assumed a known speed of sound  $C_d$  in the water column, from which the beam steering is calculated. In the real world, the sound speed varies as a function of temperature and salinity, both of which change with depth. We demonstrate this for the RR1605 sidescan data by considering the sound speed profiles collected from a set of seven expendable bathythermographs (XBTs) collected over the course of the survey. The XBT consists of a disposable sensor deployed over the side of the vessel during a transit that measures temperature as it sinks through the upper 1000 m of the water column. These measurements are used as input alongside a model of conductivity with depth to calculate the sound speed profile using Del Grosso's equations (Del Grosso 1974). Figure 7 shows the XBT profiles collected during the RR1605 cruise as well as the RMS of the XBT profiles. We expect a shallow sound velocity profile derived from an XBT to be most accurate immediately after deployment and deteriorate with time. In this way, we expect the RMS values to provide an estimate of the upper bound of sound speed error as a function of depth, at least for the duration of the cruise.

Our strategy for using these XBT data to estimate an upper bound for the displacement errors due to sound speed variations is derived from De Moustier (1988). In principle, the depth  $H$  of a point on the seafloor may be calculated as  $H(\theta) = \rho \cos \theta = (C_d/2) t \cos \theta$ , where  $C_d$  is the average

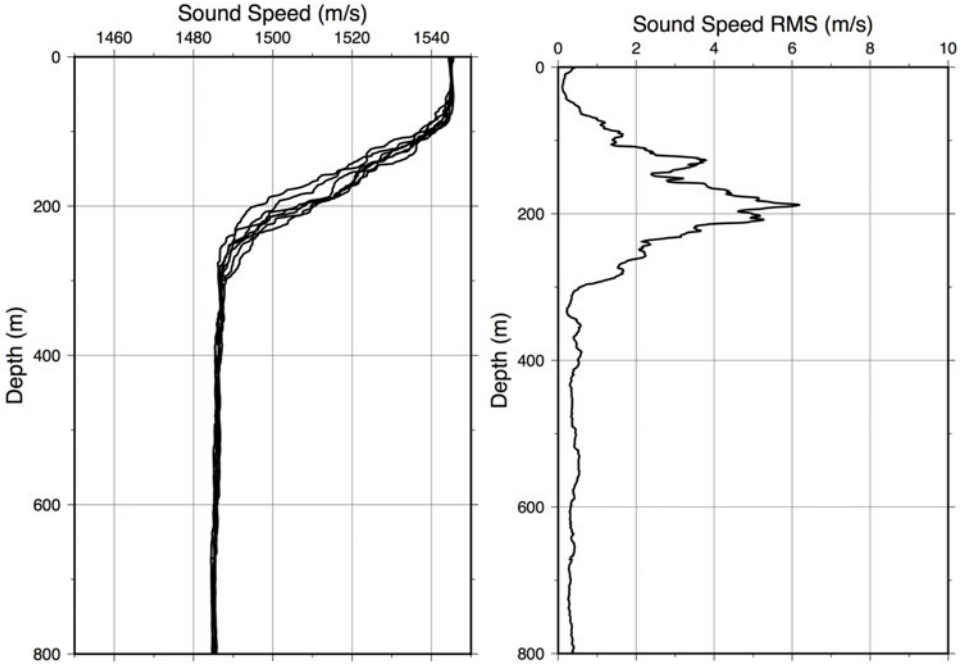


**Figure 7.** (Left) Sound speed profiles computed from XBTs deployed during the RR1605 cruise. (Right) RMS of sound speed profiles computed from XBTs deployed during the RR1605 cruise.

sound speed,  $t$  is the travel time and  $\rho$  is the slant range. This may be separated into perturbations in the surface sound speed and average sound speed profile. To demonstrate the former effect, consider the case in which the sound speed  $C_d$  is accurate except for some sound speed perturbation at the sea surface that may be measured during transit. In this case, the slant range is not affected but the apparent look angle will be bent according to Snell's Law:

$$\frac{\sin\theta'}{C'} = \frac{\sin\theta_d}{C_d} \quad (4)$$

As a result, the apparent range profile is distorted to

$$\rho'(\theta) = \frac{\rho(\theta)}{\cos\theta} \cos\left(\sin^{-1}\left[\frac{C'}{C_d} \sin\theta\right]\right). \quad (5)$$

We estimate the effect of this distortion in [Figure 8](#), which shows the percent change in range as a function of look angle calculated assuming  $C' = C_{\text{surface}} + \text{RMS}_{\text{surface}}$  using values derived from [Figure 7](#). The range difference increases for greater angles, causing greater errors for outer beams. However, this profile is symmetric about nadir, meaning that in the theoretical case of a flat seafloor, the across-track average of range measurements would be unaffected because the range errors would cancel out.

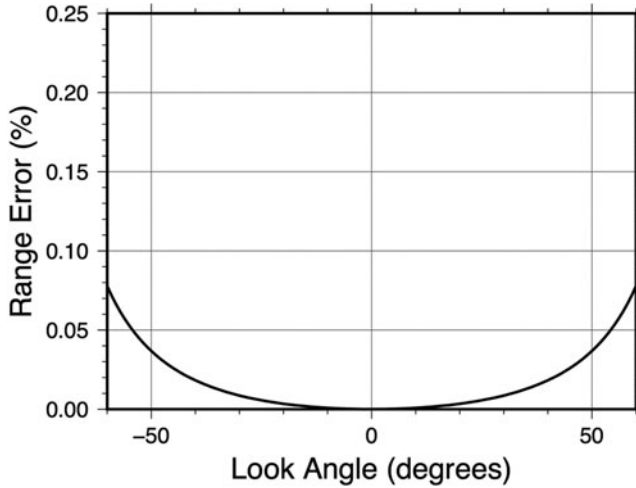


**Figure 8.** Expected uncertainty in range for the RR1605 cruise due to variations in the surface sound speed, expressed as a percent of range.

In reality, the seafloor is not completely flat; we may estimate the across-track uncertainty by multiplying the topographic relief across the swath by the percent change in range at relevant look angles. The maximum topographic relief in the RR1605 survey is  $\sim 600$  m; at a look angle of  $50^\circ$ , this corresponds to approximately 0.3 m of across-track uncertainty.

The other source of uncertainty is from errors in sound speed along the ray path from the ship to the reflector on the seafloor. Assuming sound speed depends only on depth, the strategy to address this is to consider the effect on the average speed of sound by integrating sound speed across the vertical water column, computed using the harmonic mean:

$$C_h = \left[ \frac{1}{H_0} \int_0^{H_0} \frac{dz}{C(z)} \right]^{-1}. \quad (6)$$

This will shift the range profile by a constant value since range is linear with sound speed. As a result, errors in  $C_h$  will cause uncertainty in the vertical displacement measurement. In the RR1605 cruise, we may consider the RMS of sound speed derived from XBT profiles (Figure 7) as an upper bound of the sound speed error for the duration of the cruise. Unsurprisingly, we observe the largest variance in sound speed in the region of the thermocline between 100 m and 300 m depth, due to the propagation of density waves. However, the regions shallower and deeper are far better constrained.

We estimate the variation in  $C_h$  for the duration of the cruise by computing the harmonic mean of the RMS profile. However, since the actual water depth is  $\sim 3000$  m instead of the 800 m shown in Figure 7, we must make an assumption about the sound speed variation at depth. In this case,

we assume the sound velocity conforms to models of mean annual sound velocity described by Levitus (1982) and Dushaw et al. (1993). Thus, we expect the RMS variation observed beneath the thermocline to hold constant throughout the rest of the profile. Since the region of high RMS due the thermocline is a small portion of the water column, the harmonic mean of the RMS profile is close to 0.4 m/s, being governed primarily by the stable, deep waters. If we multiply this value by the approximate two-way travel time of sound through the water column, 4 s, we arrive at an estimate of 1.6 m as the maximum RMS uncertainty in the vertical displacement measurements made during this cruise.

## Discussion and conclusions

We demonstrate displacement measurements between repeated sidescan sonar tracks collected above the Ayu Trough during the RR1605 cruise with RMS uncertainties of 0.25–0.67 m across track and 0.37–0.75 m in vertical derived from closure tests. This is sufficient to measure the displacement due to large earthquakes with  $M_w > 7.0$  or submarine slope failures. The uncertainty of these measurements has little correlation with across-track separation, demonstrating that we have successfully rotated the reference and repeat tracks into a consistent reference frame of range and azimuth. However, we were not able to successfully measure the displacement between two surveys conducted with opposite heading, which may indicate that this method only works for surveys with similar headings or that more sophisticated algorithms must be implemented to accommodate large rotations between reference frames. There is a weak dependence on the ship speed for speeds  $< 8$  knots, reflecting denser sampling on the seafloor in the azimuth direction.

For this study, we employed a simple processing strategy that fits a Gaussian peak to the correlation coefficient using a least-squares inversion. This method produces fit uncertainties on the order of 0.5 m, but the closure of Track 1 displacements imply an uncertainty closer to 0.65 m. Previous studies of digital image correlation methods have argued that more robust measurements may be obtained using a spline-fitting or Newton-Raphson algorithm (Pan et al. 2009). In addition, our correlation algorithm implicitly assumes that the ensonified seafloor is moving as two blocks, one each on the port and starboard of the vessel. Thus, localized deformation occurring in small subsections of the swath may cause the algorithm to arrive at a false solution. However, this may be mitigated by breaking the sidescan surveys into more than two subswaths as long as doing so does not significantly decrease the cross correlation factor for each subswath.

We measured displacements with magnitudes of up to 2 m over a 40 h time scale during which we expect no seafloor deformation. Thus, these measurements are probably a reflection of uncertainties introduced due to contributions from the ship navigation and sound speed profile. The contribution due to ship navigation is discussed in detail in DeSanto, Chadwell, and Sandwell (2018), and contributes 6 cm of uncertainty to the across-track measurements and 14 cm to the vertical measurements. However, use of a real-time navigation solution increases these uncertainties in ship location to the scale of many meters, compromising our ability to measure seafloor displacement with the precision required to capture phenomena such as surface displacement from offshore earthquakes.

The uncertainty contribution from the sound speed profile may be broken into three components: the contribution to the vertical uncertainty resulting from deviations of the average sound speed, the contribution to the across-track uncertainty from deviations in the surface sound speed, and horizontal variations in sound speed not measured by the XBT. Surprisingly, variation in the thermocline seems to have a limited effect on the average sound speed due to being restrained to a limited section of the water column. However, even with the current accuracy of the sound velocity in more stable portions of the water column, we still estimate a 1.6 m upper bound of uncertainty in the vertical component. This estimate depends on the two-way travel time of sound at nadir and may increase or decrease with depth accordingly. This estimate is derived from XBT measurements made in the upper water column; for deeper sound speeds we rely on the Levitus model (Levitus 1982; Dushaw et al. 1993). However, we are confident this is a reasonable assumption since we expect the sound speed to be more stable beneath the thermocline. Variation in the surface sound speed is used to estimate an across-track uncertainty of 0.3 m. This estimate depends on the topographic relief across the swath and will be minimized as the bathymetry approaches the flat seafloor assumption. However, it also is specific to the region and time of year in which the RR1605 survey was conducted. In practice, repeated surveys may be separated in time by years instead of hours. In this case, it would be prudent to collect many XBTs during both the reference and repeat surveys to obtain two estimates of sound velocity uncertainty, one for each survey.

This study was conducted with a 12 kHz multibeam sonar, but many research vessels instead employ 30 kHz multibeam sonars. The higher frequency sonar has a finer resolution but is also limited to shallower ocean depths due to greater attenuation. In deep waters, the 30 kHz multibeam can still collect bathymetry data but is limited to a narrower swath that negatively impacts the ground range resolution of sidescan, which approaches a theoretical singularity at nadir. At present, we have yet to

conduct an analogous calibration survey with a 30 kHz sonar so it is difficult to predict whether the higher frequency or narrower swath will dominate displacement measurements in deep waters. However, we expect this instrument to produce displacement measurements of sufficient, if not superior, quality at depths shallower than 1500 m.

## Acknowledgments

This paper is derived from work published in the dissertation DeSanto (2018). We would like to thank the Scripps Ship Scheduling Office, Shipboard Technical Services, James Holmes, Captain Dave Murline, and the crew of the R/V Roger Revelle, without any of whom the RR1605 cruise would not have been possible.

## Funding

This work was supported by the National Science Foundation, Marine Geology and Geophysics Division, grant 1536386. The RR1605 cruise was supported by the UC Student Ship Funds Program.

## References

- Burgmann, R., and D. Chadwell. 2014. Seafloor geodesy. *Annual Review of Earth and Planetary Sciences* 42 (1):509–534. 060313-054953.
- Caress, D. W., and D. N. Chayes. 2015. MB-System: Mapping the Seafloor. <http://www.mbari.org/data/mbsystem>, <http://www.ldeo.columbia.edu/res/pi/MB-System>. Accessed September 5, 2019.
- Davis, J. L., Y. Fialko, W. E. Holt, M. M. Miller, S. E. Owen, and M. E. Pritchard, eds. 2012. A foundation for innovation: Grand challenges in geodesy. In *Report from the Long-Range Science Goals for Geodesy Community Workshop*, 79. Boulder, Colorado: UNAVCO.
- de Moustier, C. 1988. State of the art in swath bathymetry survey systems, OED (ASME, Ocean Engineering Division). *International Hydrographic Review*, Monaco, LXV(2).
- Del Grosso, V. A. 1974. New equation for the speed of sound in natural waters (with comparisons to other equations). *The Journal of the Acoustical Society of America* 56 (4): 1084–1091.
- DeSanto, J. B. 2018. Measuring seafloor displacement using repeated sidescan sonar surveys. UC San Diego. ProQuest ID: DeSanto ucsd 0033D 17975. Merritt ID: Ark:/13030/m5ck3bpw. <https://escholarship.org/uc/item/89x555vv>. Accessed September 5, 2019.
- DeSanto, J. B., C. D. Chadwell, and D. T. Sandwell. 2018. Kinematic post-processing of ship navigation data using precise point positioning. *Journal of Navigation* 72 (3): 795–804.
- DeSanto, J. B., D. T. Sandwell, and C. D. Chadwell. 2016. Seafloor geodesy from repeated sidescan sonar surveys. *Journal of Geophysical Research: Solid Earth* 121 (7):4800–4813. 2016JB013025.



- Dushaw, B. D., P. F. Worcester, B. D. Cornuelle, and B. M. Howe. 1993. On equations for the speed of sound in seawater. *The Journal of the Acoustical Society of America* 93 (1): 255–275.
- Fujiwara, T., S. F. Christian, B. A. Katharina, S. Michael, W. Gerold, S. Tianhaozhe, K. Toshiya, and K. Shuichi. 2017. Seafloor displacement after the 2011 Tohoku-oki earthquake in the northern Japan Trench examined by repeated bathymetric surveys. *Geophysical Research Letters* 44 (23):11,833–11,839.
- Fujiwara, T., S. Kodaira, T. No, Y. Kaiho, N. Takahashi, and Y. Kaneda. 2011. The 2011 Tohoku-oki earthquake: Displacement reaching the trench axis. *Science* 334 (6060):1240.
- Fujiwara, T., K. H. Tamaki, T. Fujimoto, N. Ishii, H. Seama, K. Toh, C. Koizumi, J. Igarashi, K. Segawa, M. Kobayashi, et al. 1995. Morphological studies of the Ayu Trough, Phillippine Sea - Caroline Plate boundary. *Geophysical Research Letters* 22 (2): 109–112.
- Hong, J. K., and S. M. Lee. 2002. Reflection seismology in the southern Ayu trough, a slow-spreading divergent boundary. *Ocean and Polar Research* 24 (3):189–196.
- Kongsberg. 2011. *Kongsberg em 122 multibeam echo sounder product description*.
- Levitus, S. 1982. Climatological atlas of the world ocean. *NOAA/ERL GFDL Professional Paper* 13, Princeton, N.J., 173 pp (*Ntis PB83 - 184093*).
- Pan, B., K. Qian, H. Xie, and A. Asundi. 2009. Two-dimensional digital image correlation for in-plane displacement and strain measurement: A review. *Measurement Science and Technology* 20 (6):062001.
- Weissel, J. K., and R. N. Anderson. 1978. Is there a Caroline plate? *Earth and Planetary Science Letters* 41 (2):143–158. 821X(78)90004-3.